Angularly anisotropic correlation in granular packings

Chengjie Xia, Yixin Cao, Binquan Kou, Jindong Li, and Yujie Wang*
Department of Physics and Astronomy, Shanghai Jiao Tong University, 800 Dong Chuan Road, Shanghai 200240, China

Xianghui Xiao and Kamel Fezzaa
Advanced Photon Source, Argonne National Laboratory, 9700 South Cass Avenue, Argonne, Illinois 60439, USA
(Received 10 August 2012; revised manuscript received 26 September 2014; published 1 December 2014)

We present an x-ray microtomography study of the three-dimensional structural correlations in monodisperse granular packings. By measuring an orientation-dependent pair correlation function, we find that the local structure shows an angularly anisotropic orientation correlation. The correlation is strongest along the major axis of the local Minkowski tensor of the Voronoi cell. It turns out that this anisotropic correlation is consistent with the existence of some locally favored structures. The study suggests the importance of high-order structural correlations in random granular packings.

DOI: 10.1103/PhysRevE.90.062201 PACS number(s): 45.70.Cc, 87.59.−e

I. INTRODUCTION

The nature of random granular packings remains elusive after a significant amount of effort has been devoted to its understanding [1–4]. The difficulty lies in the lack of a generally accepted theoretical framework. In approaching the packing problem based on statistical mechanics, the theoretical efforts have been carried out mostly along two lines. A statistical volume ensemble theory was first proposed by Edwards and co-workers in which the volume takes the role of energy and the granular packing samples all mechanical stable states with equal probability [5,6]. Later, stress was augmented to simple volume ensembles and both ensembles have been extensively investigated [7–10].

Another line of work has drawn a close analogy between jammed granular packings with thermal glassy systems [11–13]. In particular, a unified jamming phase diagram has been proposed [2,11]. Recently, it was argued that the jamming transition corresponds to a glassy state at infinite pressure [13] and the jamming transition happens with a finite range of volume fractions [13,14]. Therefore, the static granular packing problem can be studied using the replica method employed in the studies of glass transitions [13].

We note that two theoretical approaches are intimately connected as the mechanical stable states in the Edwards ensemble are essentially related to the inherent states of glassy systems [5]. However, both approaches have mostly been carried out at mean-field levels. At finite dimensions, it is generally believed that fluctuations will be significant [15] and the study of the fluctuations is hampered by the fact that the concepts of order and disorder are not well defined [16,17]. Still, a jammed granular packing shows structural features that differ significantly from a "frozen" liquid state: The pair correlation function shows distinct scaling behavior around the contact peak and a split second peak structure [18–20], the distribution of contact force also shows the development of a peak in the small force regime [21], and a network of strong and weak force chains develops that shows certain correlations [22,23].

In liquid theory, the correlations can be systematically expanded by including increasingly higher orders of correlation functions [24,25]. In most cases, it is found that a simple pair correlation function is sufficient. Recent studies on the hard-sphere glass transition, which is closely related to random granular packings, have focused on the importance of high-order correlation functions including bond orientational order or locally favored structures [26–28]. There also exist approaches of systematically searching for the translational and orientational order [17]. Building upon these approaches and a recent finding that the local environment in which a particle resides is highly anisotropic [29], we characterize the orientation-dependent pair correlations beyond the standard pair correlation in three-dimensional (3D) random granular packings using synchrotron x-ray microtomography [30–32]. We found that the development of the orientation-dependent correlation is in direct correspondence with the development of some locally favored structures, especially structures with approximate fivefold symmetry [33,34]. Meanwhile, we also characterize the correlations of other parameters such as the local packing fraction and neighbor number, which also involve many-particle information [35,36].

This paper is organized as follows. In Sec. II we describe the experiment and image processing procedures. In Sec. III we introduce some indices to characterize the anisotropic Voronoi cell around each particle based on one Minkowski tensor [29,37]. We also quantify the correlations among these structural indices. In Sec. IV we define an orientation-dependent pair correlation function to quantify how local anisotropy is correlated over several particle diameters. Furthermore, we calculate an orientational entropy associated with this orientation-dependent pair correlation function. In Sec. V we introduce some correlation functions to characterize how local anisotropy indices and Voronoi cells' orientations are spatially correlated. Finally, in Sec. VI, we present a discussion and conclusion.

II. EXPERIMENT PROCEDURE

In the experiment, the bead packings were prepared by filling a 9-mm-i.d. acrylic cylindrical container to about 1cm in height using monodispersed glass beads (Duke Scientific,

*yujiewang@sjtu.edu.cn

$D = 200 \pm 15$ μm). Packings with different packing fractions were obtained by tapping the container using an electromagnetic exciter with different tapping intensity Γ, which is measured by an accelerometer as the ratio between the peak-to-peak acceleration and the gravitational acceleration. The tapping consists of a single cycle of a 60-Hz sine wave spaced with 0.5-s intervals to allow the system to relax completely. A total of 1000 taps were applied on each packing with different Γ before the tomography was carried out. The final packing fraction Φ ranges from 0.634 to 0.617 when Γ is increased from 3 to 12 [38].

The x-ray experiment was carried out at the 2BM beamline of the Advanced Photon Source at Argonne National Laboratory. The "pink" x-ray beam from a bending magnet source with a median energy around 27 keV was utilized for the high-speed tomography image acquisitions. One full tomography scan consists of 1500 projection images. The single exposure time is 30 ms and the full scan lasts about 2 min. The 3D structures were first reconstructed using the conventional filtered back-projection algorithm. Subsequently, the particles' positions and sizes were acquired by a marker-based watershed image segmentation technique [32]. The reconstructed 3D structure consists of about 17 000 particles in each packing after excluding particles within four particle diameters from the container boundary. In this following, for brevity, all physical lengths are expressed in units of average particle diameter.

III. STRUCTURAL ANISOTROPY

The local structure of the packing is ordinarily characterized by Voronoi tessellation. The local packing fraction $\Phi_{\rm loc} = w_0/w_{\rm cell}$ (w_0 and $w_{\rm cell}$ are the volumes of the particle and its Voronoi cell) and Voronoi neighbor number N (the number of particles sharing a common Voronoi cell surface with the central particle) are calculated to quantify the local environment of a granular particle. In addition to the above scalar parameters, the shape of the Voronoi cell was analyzed using a Minkowski tensor $W_1^{0,2}$ defined as the surface integral of the tensor-valued self-product of the bounding surface normal $\boldsymbol{n}$ [29,37]:

$$W_1^{0,2} = \int \boldsymbol{n} \otimes \boldsymbol{n} dA. \quad (1)$$

The tensor representation allows an explicit depiction of the cell's anisotropy. The eigenvalues of $W_1^{0,2}$ are listed as ε_1, ε_2, and ε_3 with $\varepsilon_1 > \varepsilon_2 > \varepsilon_3$ without loss of generality. To characterize the cell's shape anisotropy, the anisotropy index $\beta = \varepsilon_3/\varepsilon_1$ is introduced [29]. The value of β ranges from one (isotropic shape) to zero (a line or a plane). Additionally, another anisotropy index $\gamma = (\varepsilon_2 - \varepsilon_3)/(\varepsilon_1 - \varepsilon_3)$ is introduced to characterize the degeneracy of the three eigenvalues. The value of γ also ranges from zero (perfect oblate cell) to one (perfect prolate cell). The probability distribution functions (PDFs) of β and γ for packing with $\Phi = 0.634$ are shown in Fig. 1(a) and 1(b). The PDFs suggest that the Voronoi cells are mostly anisotropic and consist of both prolate and oblate shapes. The average β and γ for different packing fractions Φ were calculated and are shown in the insets of Figs. 1(a) and 1(b). Similar to previous findings [29], $\langle\beta\rangle$ increases for higher Φ, while $\langle\gamma\rangle$ is almost constant for different Φ.

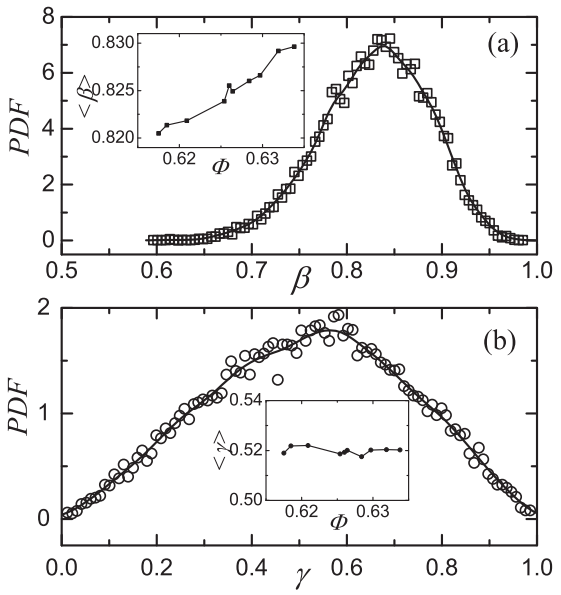

FIG. 1. Plot of the PDFs of (a) β and (b) γ for packing with $\Phi = 0.634$. The insets show the average value (a) $\langle\beta\rangle$ vs Φ and (b) $\langle\gamma\rangle$ vs Φ.

In the following, we demonstrate that β and γ are structural indices that carry local structural information of the amorphous packing beyond other standard local structural indices. In addition to the local packing fraction $\Phi_{\rm loc}$ and Voronoi neighbor number N, we calculate bond orientational order parameters Q_4 and Q_6 and three other order metrics $\Delta_{\rm fcc}$, $\Delta_{\rm hcp}$,

TABLE I. Correlation matrix for various structural indices. This matrix is symmetric, thus the data in the lower half are not shown.

	β	γ	$\Phi_{\rm loc}$	N	Q_4	Q_6	$\Delta_{\rm fcc}$	$\Delta_{\rm hcp}$	Δ_{icos}
β	1	−0.044	0.253	−0.251	−0.122	0.118	−0.049	−0.049	−0.034
γ		1	0.016	−0.019	0.014	0.080	−0.013	−0.011	−0.008
$\Phi_{\rm loc}$			1	−0.187	−0.265	0.063	−0.227	−0.290	−0.290
N				1	−0.093	−0.580	0.146	0.172	0.173
Q_4					1	0.183	0.328	0.510	0.511
Q_6						1	−0.137	−0.175	−0.181
$\Delta_{\rm fcc}$							1	0.706	0.657
$\Delta_{\rm hcp}$								1	0.990
Δ_{icos}									1

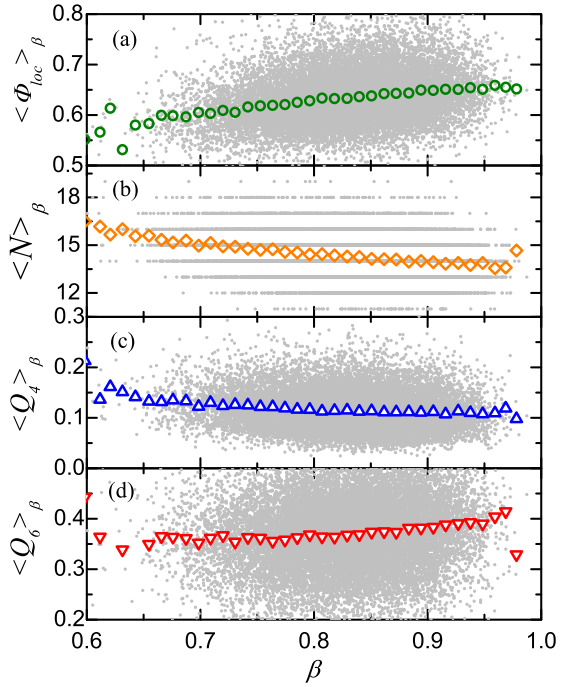

FIG. 2. (Color online) Conditional average of (a) $\Phi_{\rm loc}$, (b) N, (c) Q_4, and (d) Q_6 for given values of β. The gray scattered points are the unaveraged data points.

and Δ_{icos} [28,39]. The last three order metrics are calculated from a rank-four Minkowski tensor of a Voronoi cell, in which $\Delta_{\rm fcc}$ ($\Delta_{\rm hcp}$ or Δ_{icos}) is the root mean square of the difference between the six eigenvalues of this rank-four tensor and those of a perfect face-centered-cubic crystalline (hexagonal-close-packed or quasicrystalline icosahedral) cluster [39]. These order metrics are sensitive in identifying local crystalline clusters [39]. The linear correlation coefficients among the above structural indices for packing with $\Phi = 0.634$ are shown in Table I. We note that the anisotropy index β is correlated with $\Phi_{\rm loc}$ and N, but is almost uncorrelated with those indices quantifying local crystalline orders. Here γ seems to be uncorrelated with all other local indices. Specifically, we show the scattered plots and conditional averages of $\Phi_{\rm loc}$, N, Q_4, and Q_6 for different β in Fig. 2. The averages of all indices show monotonic dependences upon β, but the correlations are rather weak. Similar relationships apply for all other structural indices.

IV. ORIENTATIONAL CORRELATION

A. Orientation-dependent pair correlation function

In addition to β and γ, we also calculate the local orientation of each Voronoi cell from $W_1^{0,2}$. We calculate the eigenvectors corresponding to the eigenvalues of $W_1^{0,2}$: The major axis $\boldsymbol{e_M}$ and minor axis $\boldsymbol{e_m}$ correspond to ε_1 and ε_3, respectively. The global distributions of $\boldsymbol{e_M}$ and $\boldsymbol{e_m}$ are uniform in all directions, suggesting that the packing is isotropic globally. However, it turns out that the anisotropy of the Voronoi cell is not localized within the first shell, but is spatially correlated and affects the structures in a range of about three to four particle diameters around the central particle.

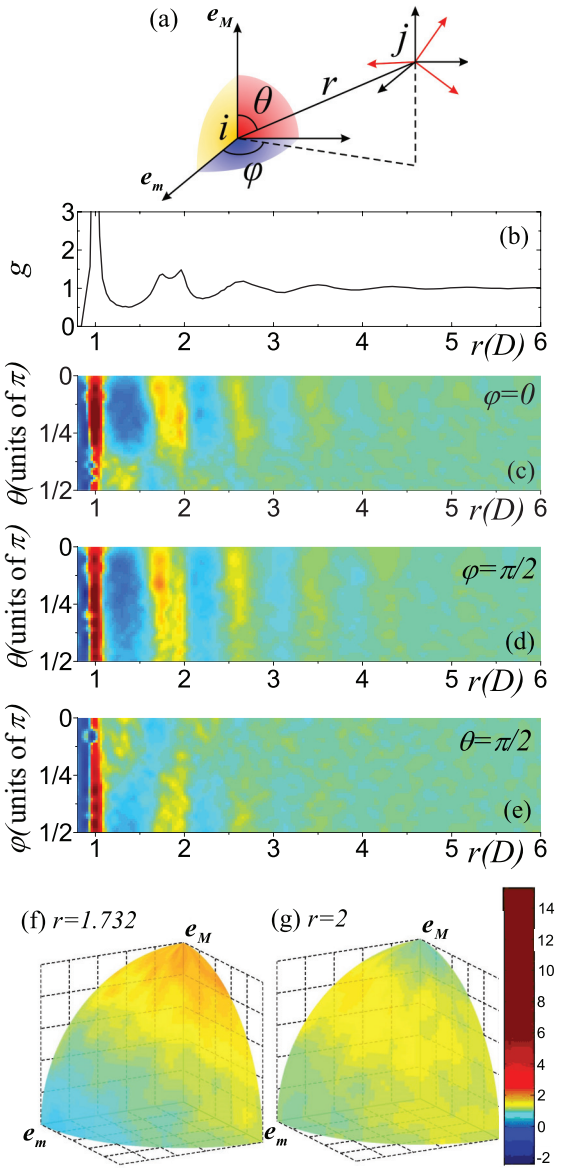

FIG. 3. (Color online) (a) Schematic for the local coordinate system of particle i and the relative position and orientation of particle j. The red coordinate system marks the orientations of the axes of particle j. (b) Ordinary pair correlation function $g(r)$. (c)–(g) Orientation-dependent pair correlation function $g(r,\theta,\varphi)$ shown on the (c) $\varphi = 0$ plane [yellow plane in (a)], (d) $\varphi = \pi/2$ plane [red plane in (a)], (d) $\theta = \pi/2$ plane [blue plane in (a)], (f) $r = \sqrt{3}$ spherical surface, and (g) $r = 2$ spherical surface.

In the following, we introduce a set of orientation-dependent correlation functions to quantify such anisotropic spatial correlations. First we augment the standard pair correlation function $g(r)$ into an orientation-dependent pair correlation function $g(r,\theta,\varphi)$. A local Cartesian coordinate system for each particle was set up based on $\boldsymbol{e_M}$ and $\boldsymbol{e_m}$: $\boldsymbol{e_M}$ is the z axis, $\boldsymbol{e_m}$ is the x axis, and $\boldsymbol{e_M} \times \boldsymbol{e_m}$ is the y axis as shown in Fig. 3(a). A local spherical coordinate system is further defined based upon the Cartesian coordinate system. In the spherical coordinate system, the relative positions and orientations of two particles' Voronoi cells can be expressed

using six independent variables: $(r_{ij},\theta_{ij},\varphi_{ij})$ represents the relative position of particle j in the coordinate system of particle i and another three variables represent the relative orientations of the two Voronoi cells.

For simplicity, we first neglect the relative orientation of two Voronoi cells and calculate an orientation-dependent pair correlation function $g(r,\theta,\varphi)$ defined as

$$g(r,\theta,\varphi) = \frac{1}{4\pi r^2 \rho \Delta r \Delta\Omega} \langle \delta(r - r_{ij})\delta(\theta - \theta_{ij})\delta(\varphi - \varphi_{ij})\rangle, \tag{2}$$

where the average is taken for all pairs of particles, ρ is the number density of the packing, Δr is the increment of r, and $\Delta\Omega$ is the size of the solid angle centering at (θ,φ). Due to the symmetry between $(\theta,\pi-\theta)$, $(\varphi,\pi-\varphi)$, and $(\varphi,-\varphi)$, we map all data to $\theta,\varphi \in [0,\pi/2]$ and average data from equivalent ranges. Since $g(r,\theta,\varphi)$ is a function with three variables, we plot it using a set of 2D colormaps as shown in Fig. 3, where different colors are used to indicate the intensity of correlations. As a comparison, the ordinary pair correlation function $g(r)$ is also plotted in Fig. 3(b). We plot $g(r,\theta,\varphi)$ on the $\varphi = 0$ plane, the $\varphi = \pi/2$ plane, and the $\theta = \pi/2$ plane. These colormaps clearly demonstrate that the pair correlation function is strongest along the major axis and weakest along the minor axis and the correlation extends to several particle diameters. Furthermore, we show $g(r,\theta,\varphi)$ at a given r [$g(r=\sqrt{3},\theta,\varphi)$ and $g(r=2,\theta,\varphi)$]. Here $r=\sqrt{3}$ and $r=2$ are chosen as the positions of two subpeaks in the split second peak of $g(r)$ [see Fig. 3(b)]. It is evident that the $r=\sqrt{3}$ peak is highest along $\boldsymbol{e_M}$ while the $r=2$ peak is relatively uniform angularly.

B. Anisotropic local configurations

In this section we try to establish the connection between the local anisotropy and its spatial correlation with some locally favored structures. As pointed out before [33], the pair correlation function $g(r)$ can be decomposed into the contributions of various local configurations, defined as jkl pairs. The jkl pairs were identified by a classification of the geometry of the common neighbors of pairs of particles. Neighboring particles (or bonded particles) were defined with a cutoff distance $r_c = 1.34$, which corresponds to the first minimum of $g(r)$. The index j corresponds to the number of neighbors common to the pair of particles. The index k is the number of bonds among the j common neighbors. The index l is the length of the longest continuous chain formed by the k bonds [33]. Motivated by this approach, we calculate the orientations of these jkl pairs and compare them with $\boldsymbol{e_M}$ and $\boldsymbol{e_m}$.

For each pair we calculate the angle θ_M (θ_m) between the pair's relative direction and the corresponding individual $\boldsymbol{e_M}$ ($\boldsymbol{e_m}$) of the two particles. Here $f_{jkl}(\theta_M)$ is the PDF of θ_M for some specific jkl types and we plot $f_{jkl}(\theta_M)/\sin\theta_M$ versus θ_M in polar coordinates as shown in Fig. 4 , where $\sin\theta_M$ is a normalization factor. Similar diagrams were also shown for θ_m. We present the results of the 555, 544, and 433 pairs corresponding to the first peak of $g(r)$ [33]. The 555 pair is a part of the icosahedral arrangement of 13 particles while the 544 and 433 pairs correspond to a part of the distorted

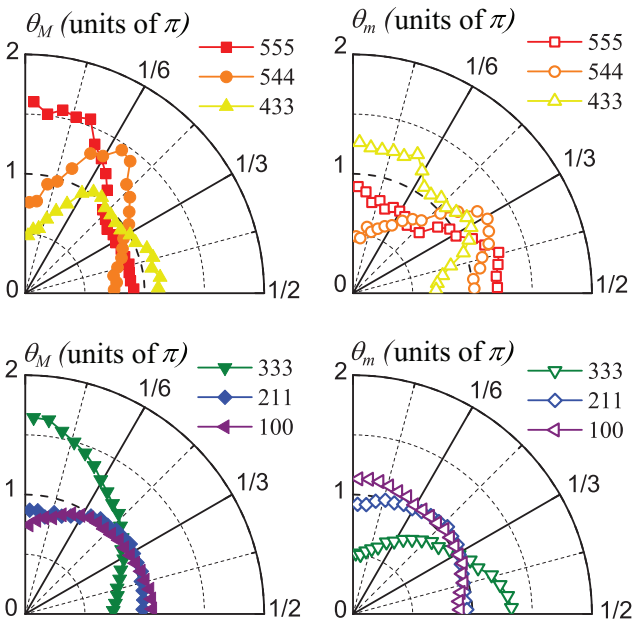

FIG. 4. (Color online) Angles between various jkl pairs and $\boldsymbol{e_M}$ (closed symbols) or $\boldsymbol{e_m}$ (open symbols). Data for the following types of pairs are shown: 555 (squares), 544 (circles), 433 (up triangles), 333 (down triangles), 211 (diamonds), and 100 (left triangles) pairs.

icosahedral order. As illustrated in Figs. 4(a) and 4(b), the 555 pair shows the best alignment with $\boldsymbol{e_M}$ compared with other pairs. We also show the results of the 333, 211, and 100 pairs, which correspond to the second peak of $g(r)$ [Figs. 4(c) and 4(d)]. The 333 pair shows the best alignment with $\boldsymbol{e_M}$ while the orientations of the other two types of pairs show comparatively uniform distributions. The 333 pair is a bipyramid cluster of two tetrahedral configurations, which is also a local dense structure and a part of the icosahedral arrangement. We note that the above 555 and 333 pairs correspond to $7A$ and $5A$ clusters in the topological cluster classification method [27]. The above calculation suggests that locally dense structures with fivefold symmetry serve as a major contribution to local anisotropy and its spatial correlations. We further verified that the choice of the cutoff distance r_c in the range [1.3,1.5] has only minor effects on above results, i.e., if neighboring particles were defined based on the Voronoi cell connection or a recent parameter-free method [40], the corresponding numbers of different particle pair types would change, but the PDFs of θ_M (θ_m) only show minor differences.

C. Orientational entropy

The anisotropic local structures of random granular packings suggest the existence of some orientational degrees of freedom. These degrees of freedom and their correlations should contribute to a nontrivial part of the configurational entropy of the packing. Motivated by the calculations of the configurational entropy for liquids with anisotropic molecules [41], we define an orientational distribution function $g_o(\theta,\varphi|r)$ according to the decomposition of $g(r,\theta,\varphi)$ into the translational and orientational parts

$$g(r,\theta,\varphi) = g_t(r) g_o(\theta,\varphi|r) \tag{3}$$

and

$$g_t(r) = \frac{1}{4\pi}\int g(r,\theta,\varphi)\sin\theta d\theta d\varphi \tag{4}$$

is the ordinary radial distribution function $g(r)$.

Then the two-particle term in the entropy expression can also be decomposed into translational and orientational parts $s = s_t + s_o$ with

$$s_t = -\frac{4\pi}{2}\rho\int [g_t(r)\ln g_t(r) - g_t(r) + 1]r^2 dr \tag{5}$$

and

$$s_o = 4\pi\rho\int g_t(r)S_o(r)r^2 dr, \tag{6}$$

where

$$S_o(r) = -\frac{1}{8\pi}\int g_o(\theta,\varphi|r)\ln g_o(\theta,\varphi|r)\sin\theta d\theta d\varphi. \tag{7}$$

In the above calculations, the Boltzmann constant is set to unity. The integration range in both Eqs. (5) and (6) is $[0,+\infty)$. In reality, a range [0,8] is sufficient. The translational and orientational entropies s_t and s_o were calculated for packing with different packing fractions as shown in Figs. 5(a) and 5(b). A decrease of both entropies with increasing packing fraction towards the random close-packing limit $\Phi \approx 0.64$ was observed [18], which suggests that the jamming transition is accompanied by increasing ordering in both translational and orientational degrees of freedom. The absolute value of s_o is about one order of magnitude smaller than that of s_t. It is worth noting that the anisotropy of a local cell is due to the multiple-particle correlations and therefore $g(r,\theta,\varphi)$ by nature corresponds to a multiple-particle to one-particle correlation. Therefore, s_o calculated from $g(r,\theta,\varphi)$ corresponds to some high-order expansion of the configurational entropy omitted in the ordinary pair correlation function $g(r)$.

Furthermore, we calculate the contributions to s_t and s_o from nearest neighbors by defining $s_{t,\mathrm{NN}}$ and $s_{o,\mathrm{NN}}$, which have an integration range [0,1.34] in Eqs. (5) and (6). We plot the relative contribution to the total entropy from nearest-neighbor particles: $s_{t,\mathrm{NN}}/s_t$ and $s_{o,\mathrm{NN}}/s_o$ as a function of Φ in the insets of Figs. 5(a) and 5(b). Particle arrangements of nearest neighbors contribute about 45% to s_o, which suggests that the orientational correlation mainly comes from the anisotropy beyond the first shell, while translational correlation beyond the first shell is comparatively smaller. Both $s_{t,\mathrm{NN}}/s_t$ and $s_{o,\mathrm{NN}}/s_o$ decrease with increasing Φ, suggesting that correlations get more long ranged towards random close packing.

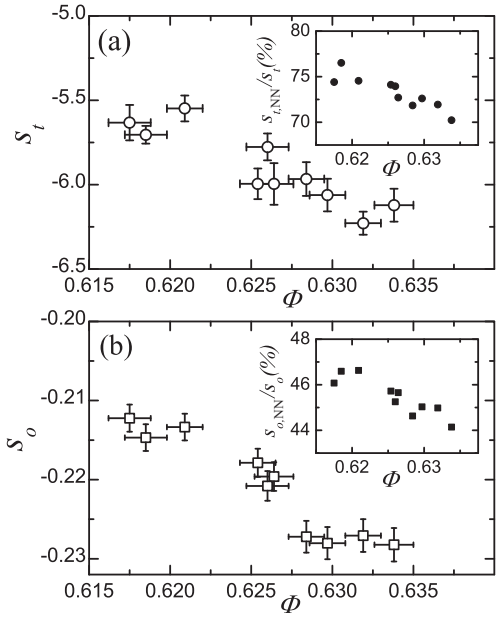

FIG. 5. (a) Translational and (b) orientational entropy for packings with different Φ. The insets show the relative contributions to (a) translational and (b) orientational entropy from nearest neighbors for packings with different Φ.

V. CORRELATION OF VORONOI CELLS

A. Correlation of cell orientation

For even higher-order orientational correlations, we focus on the spatial correlation between the orientations of eigenvectors between pairs of particles. As noted above, the correlation of particle positions is relatively strong along the major axis of $W_1^{0,2}$; we therefore presume that the mesoscale anisotropy in sphere packings mainly exists along $\boldsymbol{e_M}$. We then calculate the orientational correlation between $\boldsymbol{e_M}$ for pairs of particles and neglect the correlations of other two axes.

This orientational correlation function is defined as

$$o(r,\theta,\varphi) = \left\langle \frac{3(\boldsymbol{e_{M,i}}\cdot\boldsymbol{e_{M,j}})^2 - 1}{2}\delta(r - r_{ij})\delta(\theta - \theta_{ij})\delta(\varphi - \varphi_{ij})\right\rangle, \tag{8}$$

where the average is taken for all pairs of particles and $\boldsymbol{e_{M,i}}$ is the major axis of particle i. The $[3(\boldsymbol{e_{M,i}}\cdot\boldsymbol{e_{M,j}})^2 - 1]/2$ term is analogous to the nematic order parameter in liquid crystals. The orientational correlation function $o(r,\theta,\varphi)$ is illustrated in Fig. 6. Similar to $g(r,\theta,\varphi)$, the orientational correlation between major axes is also stronger along $\boldsymbol{e_M}$ for each particle, while the variation of $o(r,\theta,\varphi)$ for different φ seems comparatively weak. The oscillatory behavior of $o(r,\theta,\varphi)$ along $\boldsymbol{e_M}$ suggests that the orientations of $\boldsymbol{e_M}$ for neighboring particles exhibit an alternating tendency between being parallel and orthogonal to $\boldsymbol{e_M}$ of the central particle and extend to about three particle diameters. We also calculate the correlation of the orientations of minor axes of pairs of particles and find that the correlation extends to only about 1.5 particle diameters.

The estimation of configurational entropy associated with this nonuniform distribution of the orientation between $\boldsymbol{e_M}$ or even $\boldsymbol{e_m}$ is beyond the scope of this work. However, as s_o is contributed by the multiple-particle to one-particle correlation and the above $o(r,\theta,\varphi)$ correlation is contributed by multiparticle to multiparticle correlation, we presume that its contribution to the total configuration entropy should be much smaller than s_o.

B. Correlation of cell anisotropy

Finally, to fully quantify the mesoscale anisotropic structures of sphere packings, we further calculate the spatial

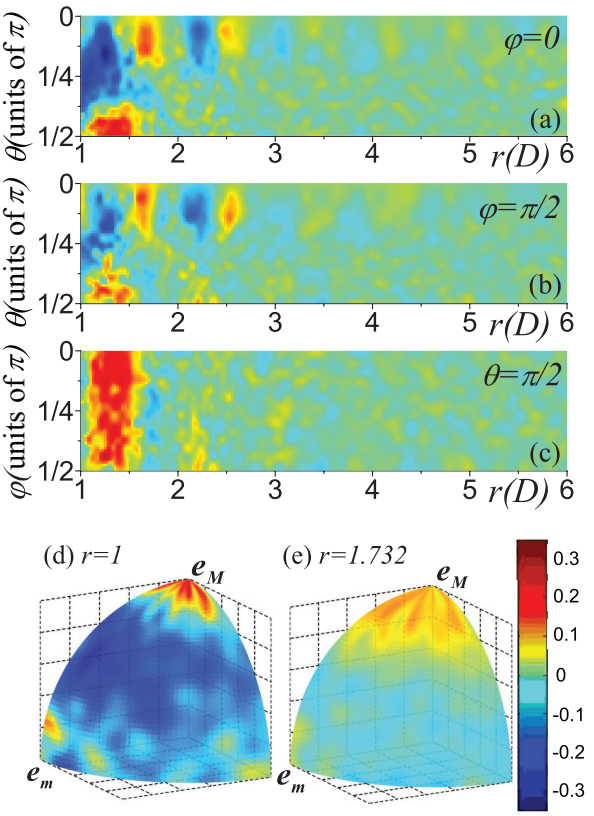

FIG. 6. (Color online) Orientation-dependent correlation function $o(r,\theta,\varphi)$ shown on the (a) $\varphi = 0$ plane, (b) $\varphi = \pi/2$ plane, (c) $\theta = \pi/2$ plane, (d) $r = 1$ spherical surface, and (e) $r = \sqrt{3}$ spherical surface.

correlations of anisotropy indices β and γ. For simplicity, we neglect the variation of spatial correlation in (θ,φ) degrees of freedom and the correlation function becomes isotropic:

$$c_a(r) = \left\langle \frac{(a_i - \langle a\rangle)(a_j - \langle a\rangle)}{\mathrm{var}(a)} \delta(r - r_{ij}) \right\rangle, \qquad (9)$$

where a represents a specific structure quantity ($a = \beta,\gamma,\Phi,N,\ldots$), the average is taken for all pairs of particles, and $\langle a\rangle$ and $\mathrm{var}(a)$ are the average value and variation of a, respectively. As shown in Fig. 7, β shows a positive correlation

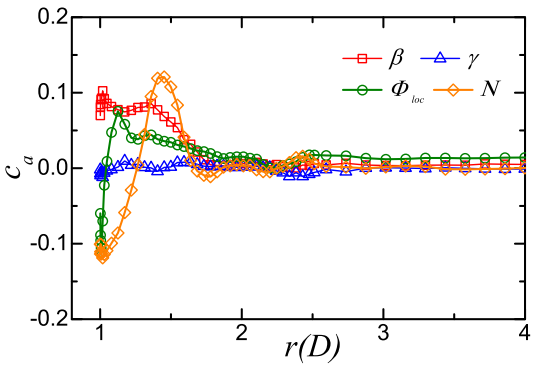

FIG. 7. (Color online) Correlation functions for various structural indices: β (squares), γ (triangles), Φ_{loc} (circles), and N (diamonds).

within two particle diameters, while the γ correlation is basically zero. This suggests that anisotropic cells tend to be located near anisotropic ones, while the degeneracy of eigenvalues seems uncorrelated. Together with the analysis of the correlation between γ and other structural quantities, it seems that whether the shape of the Voronoi cell is close to an oblate ellipsoid or a prolate one is unimportant. As a comparison we calculate $c_\Phi(r)$ and $c_N(r)$ as well (Fig. 7). It is shown that all these scalar structural parameters have a spatial correlation of about two particle diameters, which is close to the correlation length of $o(r,\theta,\varphi)$, while the correlation length of $g(r,\theta,\varphi)$ along $\boldsymbol{e}_M$ is slightly longer.

VI. DISCUSSION AND CONCLUSION

In summary, the nonuniform angular distribution of neighboring particles results in an anisotropic local structure of sphere packings. This anisotropy is well characterized through some anisotropy indices. In the current study, by using an orientation-dependent pair correlation function, we find that this anisotropy structure extends beyond first shell and shows an anisotropic correlation extending to several particle diameters with the maximum correlation along the major axis of the local Minkowski tensor.

The current study bridges the approaches of studying the packing structure using a topological classification [27] and systematic expansion beyond pair correlation functions [24]. By decomposing the standard pair correlation function into translational and orientational parts, we were able to investigate their individual contributions to the correlations in the system and have clearly established the connection to the topological structural analysis.

However, there are two points that need caution. The first is that the preferred correlation along the major axis only suggests a strong correlation along a fixed direction while in reality the true correlation in amorphous systems might not follow a straight line [42]. Therefore, the actual correlation could be even longer. Second, in defining the neighbors, the method of a cutoff distance has been adopted that follows the custom in systems with short-range attractive interactions in which the local cluster structures correspond to the local minima of the energy landscape [27]. For hard-sphere systems, the interactions are purely repulsive. Therefore, how to establish the connections between local anisotropy, particular local structures, and their free-energy implications remains elusive.

The current study also presents interesting connections with packings of anisotropic particles, which have orientational degrees of freedom intrinsically [43,44]. Additionally, the local anisotropic correlations could also be related to force chains [22,23]. How to relate the structure with force information will be of great interest in the future.

ACKNOWLEDGMENTS

We appreciate helpful discussion with Yuliang Jin. The use of the Advanced Photon Source was supported by the US Department of Energy, Office of Science, Office of Basic Energy Sciences, under Contract No. DE-AC02-06CH11357.

Some of the preliminary experiments were carried out at the BL13W1 beamline of the Shanghai Synchrotron Radiation Facility. The work was supported by the National Natural Science Foundation of China through Grant No. 11175121, National Basic Research Program of China (973 Program No. 2010CB834301).

[1] J. Bernal and J. Mason, Nature (London) **188**, 910 (1960).
[2] A. J. Liu and S. R. Nagel, Annu. Rev. Condens. Matter Phys. **1**, 347 (2010).
[3] S. Torquato and F. Stillinger, Rev. Mod. Phys. **82**, 3197 (2010).
[4] M. P. Ciamarra, P. Richard, M. Schröter, and B. P. Tighe, Soft Matter **8**, 9731 (2012).
[5] S. F. Edwards and R. Oakeshott, Physica A **157**, 1080 (1989).
[6] A. Mehta and S. Edwards, Physica A **157**, 1091 (1989).
[7] S. F. Edwards and D. V. Grinev, Phys. Rev. Lett. **82**, 5397 (1999).
[8] R. C. Ball and R. Blumenfeld, Phys. Rev. Lett. **88**, 115505 (2002).
[9] S. Henkes and B. Chakraborty, Phys. Rev. Lett. **95**, 198002 (2005).
[10] H. A. Makse and J. Kurchan, Nature (London) **415**, 614 (2002).
[11] A. J. Liu and S. R. Nagel, Nature (London) **396**, 21 (1998).
[12] R. D. Kamien and A. J. Liu, Phys. Rev. Lett. **99**, 155501 (2007).
[13] G. Parisi and F. Zamponi, Rev. Mod. Phys. **82**, 789 (2010).
[14] P. Chaudhuri, L. Berthier, and S. Sastry, Phys. Rev. Lett. **104**, 165701 (2010).
[15] Y. Jin, J. G. Puckett, and H. A. Makse, Phys. Rev. E **89**, 052207 (2014).
[16] S. Torquato, T. M. Truskett, and P. G. Debenedetti, Phys. Rev. Lett. **84**, 2064 (2000).
[17] T. M. Truskett, S. Torquato, and P. G. Debenedetti, Phys. Rev. E **62**, 993 (2000).
[18] C. S. O'Hern, L. E. Silbert, A. J. Liu, and S. R. Nagel, Phys. Rev. E **68**, 011306 (2003).
[19] A. Donev, S. Torquato, and F. H. Stillinger, Phys. Rev. E **71**, 011105 (2005).
[20] L. E. Silbert, A. J. Liu, and S. R. Nagel, Phys. Rev. E **73**, 041304 (2006).
[21] C. S. O'Hern, S. A. Langer, A. J. Liu, and S. R. Nagel, Phys. Rev. Lett. **86**, 111 (2001).
[22] T. S. Majmudar and R. P. Behringer, Nature (London) **435**, 1079 (2005).
[23] F. Radjai, D. E. Wolf, M. Jean, and J.-J. Moreau, Phys. Rev. Lett. **80**, 61 (1998).
[24] J.-P. Hansen and I. R. McDonald, *Theory of Simple Liquids*, 2nd ed. (Academic, New York, 1990).
[25] D. C. Wallace, J. Chem. Phys. **87**, 2282 (1987).
[26] H. Tanaka, T. Kawasaki, H. Shintani, and K. Watanabe, Nat. Mater. **9**, 324 (2010).
[27] C. P. Royall, S. R. Williams, T. Ohtsuka, and H. Tanaka, Nat. Mater. **7**, 556 (2008).
[28] P. J. Steinhardt, D. R. Nelson, and M. Ronchetti, Phys. Rev. B **28**, 784 (1983).
[29] G. E. Schröder-Turk, W. Mickel, M. Schröter, G. W. Delaney, M. Saadatfar, T. J. Senden, K. Mecke, and T. Aste, Europhys. Lett. **90**, 34001 (2010).
[30] P. Richard, P. Philippe, F. Barbe, S. Bourlès, X. Thibault, and D. Bideau, Phys. Rev. E **68**, 020301(R) (2003).
[31] T. Aste, M. Saadatfar, and T. Senden, Phys. Rev. E **71**, 061302 (2005).
[32] Y. X. Cao, B. Chakrabortty, G. C. Barker, A. Mehta, and Y. J. Wang, Europhys. Lett. **102**, 24004 (2013).
[33] A. S. Clarke and H. Jónsson, Phys. Rev. E **47**, 3975 (1993).
[34] A. V. Anikeenko and N. N. Medvedev, Phys. Rev. Lett. **98**, 235504 (2007).
[35] T. Aste and T. Di Matteo, Eur. Phys. J. E **22**, 235 (2007).
[36] S. C. Zhao, S. Sidle, H. L. Swinney, and M. Schröter, Europhys. Lett. **97**, 34004 (2012).
[37] G. E. Schröder-Turk, W. Mickel, S. C. Kapfer, M. A. Klatt, F. M. Schaller, M. J. F. Hoffmann, N. Kleppmann, P. Armstrong, A. Inayat, D. Hug, M. Reichelsdorfer, W. Peukert, W. Schwieger, and K. Mecke, Adv. Mater. **23**, 2535 (2011).
[38] E. R. Nowak, J. B. Knight, M. L. Povinelli, H. M. Jeager, and S. R. Nagel, Powder Technol. **94**, 79 (1997).
[39] S. C. Kapfer, W. Mickel, K. Mecke, and G. E. Schröder-Turk, Phys. Rev. E **85**, 030301 (2012).
[40] Z. A. Tian, R. S. Liu, K. J. Dong, and A. B. Yu, Europhys. Lett. **96**, 36001 (2011).
[41] T. Lazaridis and M. Karplus, J. Chem. Phys. **105**, 4294 (1996).
[42] T. Tomida and T. Egami, Phys. Rev. B **52**, 3290 (1995).
[43] A. Donev, I. Cisse, D. Sachs, E. A. Variano, F. H. Stillinger, R. Connelly, S. Torquato, and P. M. Chaikin, Science **303**, 990 (2004).
[44] C. Xia, K. Zhu, Y. Cao, H. Sun, B. Kou, and Y. Wang, Soft Matter **10**, 990 (2014).